Biological Procedures Online

RESEARCH

Open Access

Metabolic and Immunological Implications of MME$^+$CAF-Mediated Hypoxia Signaling in Pancreatic Cancer Progression: Therapeutic Insights and Translational Opportunities

Bin Wang[1†], Yue Pan[2†], Yongjie Xie[3†], Cong Wang[1], Yinli Yang[1], Haiyan Sun[1], Zhuchen Yan[1], Yameng Cui[1], Ling Li[1], Yaoyao Zhou[5*], Weishuai Liu[4*] and Zhanyu Pan[1*]

Abstract

Pancreatic cancer is a devastating malignancy with a high mortality rate, poor prognosis, and limited treatment options. The tumor microenvironment (TME) plays a crucial role in tumor progression and therapy resistance. Multiple subpopulations of cancer-associated fibroblasts (CAFs) within the TME can switch between different states, exhibiting both antitumorigenic and protumorigenic functions in pancreatic cancer. It seems that targeting fibroblast-related proteins and other stromal components is an appealing approach to combat pancreatic cancer. This study employed single-cell transcriptome sequencing to identify MME (Membrane Metalloendopeptidase)-expressing CAFs in pancreatic cancer. Systematic screening was conducted based on tumor differentiation, lymph node metastasis, and T-stage parameters to identify and confirm the existence of a subpopulation of fibroblasts termed MME$^+$CAFs. Subsequent analyses included temporal studies, exploration of intercellular communication patterns focusing on the hypoxia signaling pathway, and investigation of MME$^+$CAF functions in the pancreatic cancer microenvironment. The pathway enrichment analysis and clinical relevance revealed a strong association between high MME expression and glycolysis, hypoxia markers, and pro-cancer inflammatory pathways. The role of MME$^+$CAFs was validated through in vivo and in vitro experiments, including high-throughput drug screening to evaluate potential targeted therapeutic strategies. Single-cell transcriptome sequencing revealed tumor-associated fibroblasts with high MME expression, termed MME$^+$CAF, exhibiting a unique end-stage differentiation function in the TME. MME$^+$CAF involvement in the hypoxia signaling pathway suggested the potential effects on pancreatic cancer progression through intercellular communication. High MME expression was associated with increased glycolysis, hypoxia markers (VEGF), and pro-cancer inflammatory pathways in pancreatic cancer patients, correlating

[†]Bin Wang, Yue Pan, and Yongjie Xie are co-first authors of this paper.

*Correspondence:
Yaoyao Zhou
1457893602@qq.com
Weishuai Liu
liuweishuai@126.com
Zhanyu Pan
panzhanyu@tjmuch.com

Full list of author information is available at the end of the article

with lower survival rates, advanced disease stage, and higher oncogene mutation rates. Animal experiments confirmed that elevated MME expression in CAFs increases tumor burden, promotes an immunosuppressive microenvironment, and enhances resistance to chemotherapy and immunotherapy. The developed MME^{+}CAF inhibitor IOX2 (a specific prolyl hydroxylase-2 (PHD2) inhibitor), combined with AG (Paclitaxel + Gemcitabine) and anti-PD1 therapy, demonstrated promising antitumor effects, offering a translational strategy for targeting MME in CAFs of pancreatic cancer. The study findings highlighted the significant role of MME^{+}CAF in pancreatic cancer progression by shaping the TME and influencing key pathways. Targeting MME presented a promising strategy to combat the disease, with potential implications for therapeutic interventions aimed at disrupting MME^{+}CAF functions and enhancing the efficacy of pancreatic cancer treatments.

Keywords Pancreatic cancer, Fibroblasts, Hypoxia, IOX2, Anti-PD1

Introduction

Pancreatic cancer is characterized by its aggressive nature and poor prognosis [1, 2], with the TME playing a crucial role in disease progression [3–5]. Despite advancements in cancer research, pancreatic cancer patients have short survival time because it is often diagnosed in advanced stages and therapeutic challenges [6, 7]. Amongst the various components of the TME, CAFs have gained significant attention [8, 9]. The complex network of interactions within the TME plays a crucial role in the enigmatic landscape of pancreatic cancer. Within this TME, CAFs exert significant control over the progression of the disease and the effectiveness of treatment [10, 11]. These stromal cells play a multifaceted role in shaping the TME, orchestrating protumorigenic signaling pathways, and fostering immune evasion mechanisms [12–14].

A defining feature of pancreatic cancer is its aberrant metabolic profile, characterized by enhanced glycolytic activity through the Warburg effect [15, 16]. This shift towards aerobic glycolysis not only fuels tumor growth and metastasis but also contributes to immune suppression within the TME, posing a significant barrier to successful therapeutic interventions [17]. Recent studies have highlighted the intricate interplay between CAFs and metabolic reprogramming, particularly focusing on glycolysis [18–20]. Glycolysis, the process through which glucose is metabolized to generate energy, has emerged as a key metabolic pathway that fuels the rapid proliferation of cancer cells [21]. Becker et al.. demonstrated that CAFs exhibit a pro-glycolytic phenotype, which helps to fuel the metabolism of breast cancer cells and enhances tumor growth [22]. CAFs in tumor stroma tend to activate both glycolysis and autophagy in contrast to neighboring cancer cells, which leads to a reverse Warburg effect [23]. CAFs underwent a reverse Warburg effect when co-cultured with pancreatic cancer cells, represented by enhanced aerobic glycolytic metabolism. Nevertheless, Shikonin (specific pyruvate kinase M2 inhibitor) reduced aerobic glycolysis in CAFs by reducing their glucose uptake and glycolytic protein expression [24]. Understanding the relationship between CAFs and glycolysis in pancreatic cancer may provide novel insights into the development of targeted therapeutic strategies to disrupt the metabolic dependencies of tumor cells [25]. In this context, elucidating the molecular mechanisms underlying the crosstalk between CAFs and glycolysis holds promise for improving therapeutic outcomes and survival in patients with pancreatic cancer.

In parallel, the immunosuppressive milieu within pancreatic tumors poses a significant hurdle to effective immunotherapeutic strategies [26]. Regulatory T-cells [27], myeloid-derived suppressor cells [28, 29], and other immune checkpoints [30] conspire to dampen antitumor immune responses, fostering a tolerogenic microenvironment that facilitates disease progression and limits the efficacy of immune-based interventions. The convergence of CAF-driven tumorigenic signals and immune evasion mechanisms underscores the importance of understanding the dynamic interplay between these elements in shaping the pancreatic cancer microenvironment [31]. Unraveling the complexities of CAF-mediated immunosuppression is paramount for devising innovative therapeutic approaches that target both the stromal and immune compartments, offering new avenues for intervention in this challenging disease [32]. It has been reported that lactic acid in the highly glycolytic TME acts as a regulatory factor for the function of regulatory T-cells (Tregs) in the TME by increasing the expression of PD-1 [33]. Aerobic glycolysis promotes HK2-dependent PD-L1 expression and subsequent immune evasion using cultured brain tumor cells [17]. High glucose condition in the TME promotes immune suppression by upregulating glycolysis in pancreatic cancer cells, which can be rescued via knockdown Bmi1 expression or after 2-deoxy-D-glucose treatment [34]. JQ1 combats PDT (Photoimmunotherapy by photodynamic therapy)-mediated immune evasion by inhibiting the expression of c-Myc and PD-L1, which are key regulators of pancreatic cancer glycolysis and immune evasion [35]. The challenge lies in unraveling the intricate crosstalk between these key players-CAFs, glycolytic pathways, and immune checkpoints—in the context of pancreatic cancer to develop synergistic treatment strategies that overcome therapeutic resistance and improve patient outcomes [36, 37]. This study aims

to analyze the molecular mechanisms that underlie these interactions to identify vulnerabilities within the TME that can be leveraged for therapeutic purposes [38].

MME, also known as Neprilysin, CD10, or Neutral Endopeptidase, encodes for enkephalinase [39, 40]. This transmembrane metalloprotease is widely expressed in various tissues and organs including the brain, kidney, heart, liver, etc. Its molecular structure comprises an extracellular N-terminus, transmembrane region, and cytoplasmic C-terminus, playing a role in neurotransmitter degradation, metabolic regulation (e.g., hormone concentration regulation), immune response, and holds significant importance in drug development, disease relevance (e.g., Alzheimer's disease, hypertension, cancer), as well as cancer research and neuroscience [40–43]. MME is a zinc peptidase that belongs to the M13 family of cell-surface peptidases. This family also includes endothelin converting enzymes (ECE-1 and ECE-2), KELL, and PEX. MME cleaves peptide bonds on the amino side of hydrophobic amino acids and is the key enzyme in the processing of a variety of physiologically active peptides. In breast cancer, fibroblasts can be classified into nine clusters, with the tCAFS (tumor-like CAFs) cluster in particular exhibiting high levels of MME and PDPN, among other markers. In addition, single-cell analyses of lung cancer have reported high expression of MME specific to hypoxia-tCAF and tCAF [44, 45].

This study employs a combination of single-cell transcriptome sequencing, clinical data analysis, and functional experiments to elucidate the molecular mechanisms underlying the protumorigenic properties of MME^{+}CAF. The involvement of MME^{+}CAF in the hypoxia signaling pathway suggests potential effects on pancreatic cancer progression through intercellular communication. High MME expression is associated with increased glycolysis, hypoxia markers (VEGF), and pro-cancer inflammatory pathways in pancreatic cancer patients. The findings reveal a distinct gene expression profile and signaling pathways associated with MME^{+}CAF, highlighting its potential as a therapeutic target in pancreatic cancer. Through a comprehensive analysis of patient samples and preclinical models, the study demonstrates that MME^{+}CAF abundance correlates with disease progression, immune dysregulation, and poor clinical outcomes in pancreatic cancer. Furthermore, the study identifies potential therapeutic strategies targeting MME^{+}CAF, offering new avenues for improving treatment efficacy and patient survival.

In conclusion, this study provides insights into the complex interplay between CAFs and pancreatic cancer, emphasizing the significance of MME^{+}CAF in driving tumor progression and therapeutic resistance. By unraveling the functional properties of MME^{+}CAF, this study aims to pave the way for the development of precision medicine approaches tailored to disrupt the TME and enhance treatment outcomes in pancreatic cancer.

Materials and Methods

Surgical Samples and Demographics of Participants

The Cancer Institute of Tianjin Medical University and the Hospital Ethics Committee (bc20240074) approved the use of all samples and participants' information. All participants provided written consent for the use of their samples and disease information for future investigations according to the ethics committee and in accordance with the recognized ethical guidelines of Helsinki.

Sorting of Human and Murine CAFs

The Ethics Committee approved the acquisition of all human PDAC samples from the Pancreatic Cancer Department of Tianjin Medical University Cancer Institute & Hospital. These samples were collected with the informed consent of the donors. The clinical information of participants whose tumors were used for isolating CAFs is presented in Table S1. Human pancreatic CAFs were isolated from fresh PDAC surgical samples using a culture outgrowth approach. Specifically, fresh human PDAC surgical samples were sliced into blocks of 1–3 mm using a sharp blade. These blocks were subsequently seeded in 6-cm culture dishes and cultivated with DMEM medium supplemented with 10% fetal bovine serum. After 7–15 days, when the cell confluence reached 90%, CAFs were subjected to trypsinization, replated into another culture plate, and further cultured with a complete DMEM medium. The isolated cells were identified using immunofluorescence and FCM, showing positivity for the following mesenchymal-specific markers: Desmin, Collagen I, and α-SMA, and negativity for other cell lineage markers: CD326 for epithelial cells, CD31 for endothelial cells, and CD45 for immune cells. The human PDAC cell line SW1990 was kindly provided by Prof. Keping Xie (MD Anderson Cancer Center, Houston, TX) and was maintained in RPMI-1640 with 10% FBS.

Screening of Primary Resting Fibroblasts from Human and Murine Sources

(1) The pancreas of mice was removed and cut into small pieces and rinsed with PBS; then the floating fat was removed. (2) Digestion: 0.02% collagenase IV, 0.02% pronase, and 0.05 DNAse were added to the enzyme dilution to a final volume of 10 ml. 3). The digestive enzymes and tissue samples were mixed evenly and incubated in a 37 °C water bath for 12–15 min. 4). Then 10 ml of complete medium was introduced to the aforementioned volume to counteract the digestion and subsequently underwent filtration using a 100-μm filter. 5) The resulting mixture was centrifuged at 450 g for 7 min.

Subsequently, the supernatant was removed, and 5 ml of 15% optiprep (1.25 ml optiprep+3.75 ml tris base-NaCl) was added. The tube wall was gently brushed with 5 ml of 11.5% optiprep (0.96 ml optiprep+4.04 ml tris base-NaCl), and 5 ml of GBSS was gently brushed along the tube wall. 6) Then it was centrifuged at 1400 g for 17 min and the white film layer between GBSS and 11.5% optiprep was collected. 7) The collected white film layer was re-suspended and washed with GBSS, centrifuged at 450 g for 8 min, and cultured in a complete DMEM medium.

ScRNA-Sequencing Dta Processing

The 10X Genomics-based scRNA data for 35 PAAD samples were downloaded from the Genome Sequence Archive (CRA001160). A total of 57,004 cells were annotated and distinct cell clusters were identified using representative markers. The default parameters of the "Seurat" package were utilized, and the harmony algorithm was employed to de-batch the data. Subsequently, the Uniform Manifold Approximation and Projection (UMAP) technique was applied to reduce the dimensionality and visualize the cell subpopulations. The differentially expressed genes (DEGs) were compared among cell clusters with the Seurat 'FindAllMarkers' function. The fibroblasts were divided into seven subpopulations according to highly expressed genes. The "CellChat" package was used to infer and analyze cellular communication from the PAAD scRNA-seq data. The pseudo-time evolutionary trajectory was inferred from the Slingshot method.

Development of RNA-Sequencing Library

The strand-specific libraries were developed by using the TruSeq Stranded mRNA Sample Prep Kit (Illumina), according to the manufacturer's instructions. Poly-adenylated RNA from intact total RNA was refined using oligo-dT beads. The extracted complementary DNA fragment was ligated to Illumina paired-end sequencing adapters, 3′ ends adenylated and amplified by PCR. The libraries were sequenced with 65-base pair (bp) single-end reads on a HiSeq 2500 System in high output mode using V4 chemistry (Illumina). Gene expression levels were quantified by Salmon (see URLs) using default parameters for both applications after raw reads were aligned to GRCh38 using a STAR RNA-seq aligner.

Genomic Mutation Analysis

The somatic mutations in the Mutation Annotation Format (MAF) file for all the PAAD patients were obtained from the TCGA cohort. Maftools is agnostic of bigger alignment files and simply requires somatic variations in MAF [46]. It provides many analysis and visualization modules, including driver gene identification, signature, pathway, enrichment, and association analyses, that are frequently used in cancer genomic investigations. This study employed the R Bioconductor package "Maftools" package to analyze and visualize PAAD genomic mutation data. The "Forestplot" package was also used to compare genes with significant mutation frequency differences between the two groups.

Analysis of Immune Cell Infiltration

The GSVA scoring system was employed to calculate the infiltration scores of highly expressed genes in MME^{+}CAF for each sample in the bulk transcriptome to determine the MME^{+}CAF infiltration scores. Based on the median of the infiltration scores, they were categorized into high and low groups. A diverse array of algorithms, such as TIMER, CIBERSORT, CIBERSORT-ABS, EPIC, MCPCOUNTER, XCELL, and QUANTISEQ, were implemented to quantify immunoreactivity to compare the immune microenvironment of high and low MME^{+}CAF infiltration groups. The degree of correlation between MME^{+}CAF and immune cells was calculated using Pearson correlation analysis. The TIDE algorithm was also employed to evaluate the immune exclusion score, immune dysregulation score, and total TIDE score in different groups.

Prediction of Drug Sensitivity of MME^{+} Fibroblast

The cell line expression data were obtained from the Genomics of Drug Sensitivity in Cancer (GDSC) database (https://www.cancerrxgene.org/). The IC_{50} value matrix was also included for drug sensitivity analysis. The "oncopredict" R package was employed to generate predictive drug sensitivity data (IC50) for pancreatic cancer samples. The Connectivity map analysis (CMap) online tool (http://clue.io) has been verified to be useful in silico drug screening tools to target disorders. The genes positively correlated with MME^{+}fibroblasts were subjected, and the query result was a list of drugs with a "connectivity score" ranging from +1 (positive connectivity) to -1 (negative connectivity).

Cell Culture and Transfection

Primary CAFs were isolated from invasive pancreatic ductal adenocarcinoma samples obtained from surgery or KPC genetic engineering mice. The KPC mice were primarily 10 weeks old and were initially identified through PCR for KRAS-TP53 mutations, and subsequently through in vivo ultrasound for tumorigenesis and tumor burden. Briefly, tissues were digested by collagenase type I, collagenase type III, and hyaluronidase (1.5 mg/ml) at $37^{\circ C}$ with agitation for 2–3 h in DMEM with 10% FBS. Subsequently, the dissociated tissues were incubated at room temperature for 5 minutes without shaking to isolate primary fibroblasts. Then the stromal

cell-enriched supernatant was removed and transferred to a new tube. Human fibroblasts were then cultured in DMEM with 10% FBS and the purity of fibroblasts was validated by flow cytometry analysis. CAFs from passages 2 to 10 were used for subsequent experiments [47]. To introduce genetic material into CAFs, a total of 1×10^5 CAFs were placed in each well of 6-well plates. Lentiviral particles with a multiplicity of infection (MOI) of 100 were added to the CAFs, along with 5 μg/mL of Polybrene. The CAFs were then incubated with these substances for 12 h. To transduce mouse fibroblasts, 5×10^5 cells per well were treated with mouse MME-overexpression lentiviral particles (MOI of 20) and 5 μg/mL Polybrene for 12 h in 6-well plates. The human pancreatic cancer cell line (SW1990) and the murine pancreatic cancer cell line (PANC02) were cultured on RPMI1640 and DMEM media supplemented with 10% Fetal Bovine Serum (FBS), 100 U of penicillin, and 100 μg/ml streptomycin at 37 in a humidified atmosphere of 95% air and 5% CO_2.

Western Blot

Cells were lysed using RIPA lysis mixed with phosphatase inhibitors and protease inhibitors. Protein concentrations were measured by BCA protein assay. The same amount of protein was separated by sodium dodecyl sulfate-polyacrylamide gel electrophoresis (SDS-PAGE). Related antibodies were diluted at 1:1000 and incubated overnight at 4 °C with membranes containing blot proteins. Horseradish peroxidase-conjugated goat anti-rabbit antibody and goat anti-mouse antibody were diluted at a ratio of 1:5000 as secondary antibodies. The blots were detected with a Chemi-Scope exposure machine. We have added the concentration and source of the protein in Table S2.

qPCR

Total RNA was extracted from pancreatic cancer cell lines using TRIzol reagent. Then, the mRNA was used for first-strand cDNA synthesis with the Reverse Transcription PCR System (Bimake) according to the manufacturer's instructions. RT-PCR was performed to measure the mRNA levels of the target genes. Each RT-PCR experiment was repeated independently at least three times. β-Actin was also used as a loading control. The primers information was supplemented in the Table S3.

Flow Cytometry

Flow cytometry is mainly based on mouse-derived sorted CAF and KPC cell lines mixed and injected subcutaneously into immunocompetent mice to form tumors. The tissues contain KPC cells, CAFs, and many immune cells. For mouse tumor tissues, samples were prepared into a single-cell suspension. The harvested cells were divided into separate tubes for each antibody staining. After adding appropriate concentrations of fluorochrome-conjugated antibodies, the mixture was incubated for 30 min away from light. The above samples were detected using a Beckman flow cytometer and the obtained data were analyzed in software Flow Jo-10.0.

Multiplex Fluorescent IHC

The development of multiplex fluorescent IHC is mainly carried out after subcutaneous tumor formation by mixed injection of mouse-derived CAF and mouse-derived KPC cell lines for sectioning. In brief, 5 μm of PDAC slides were deparaffinized and rehydrated through a graded series of ethanol solutions (100% 1×10 min; 100% 2×10 min; 95%×10 min; and rinsed in 70%) before antigen retrieval in heated Citric Acid Buffer (pH 6.0) in microwave treatment for 15 min (EZ Retriever microwave). Each slide was put through the process of staining including a protein block with blocking buffer followed by primary antibody targeting Ki67 and corresponding secondary HRP-conjugated polymer. Each HRP-conjugated polymer mediated the covalent binding of a different fluorophore for signal amplification. Ki67 was labeled by Opal 690(676–694 nm). This reaction was followed by additional antigen retrieval in a heated Citric Acid Buffer (pH 6.0) for 15 min to remove bound antibodies. DAPI was used to identify nuclei, and slides were mounted with a fluorescence mounting medium. All analyses were conducted with the same type of control. Images were captured by the Zeiss fluorescence microscope (400×) and analyzed in ImageJ.

TUNEL Staining Assay

The tumor tissues were fixed in formalin, embedded in paraffin, and cut into sections of 5 μm. TUNEL assay was used to detect apoptosis in the tumor tissues according to the manufacturer's protocol. Tissue sections were analyzed to detect the localized green fluorescence of apoptotic cells, and DAPI was used to visualize the cell nuclei. Finally, images were captured by the Zeiss fluorescence microscope (400×) and analyzed in ImageJ.

Extracellular Acidification rate (ECAR) and Oxygen Consumption rate (OCR)

Seahorse XF96 Extracellular Flux Analyzer was used to detect cellular ECAR and OCR. On the first day, experimental and control cells were seeded into Seahorse XF96 cell culture microplates, and the XFe96 sensor cartridges were hydrated. At least 5 replicates were performed for the measurement of each group. A day later, microplates were incubated with a basic culture medium (containing 1 mM L-glutamine, without glucose) for 1 h before the assay was conducted to detect ECAR. Then ECAR was measured with the sequential injection of glucose, oligomycin, and 2-deoxyglucose (final concentration: 10

mM, 1 μM, and 50 mM respectively). For OCR detection, microplates were incubated with a basic culture medium (17 mM glucose, 1 mM sodium pyruvate, 2 mM L-glutamine, pH: 7.4) for 1 h before the assay. OCR was then measured with the sequential injection of Oligomycin, FCCP, and Rotenone/Antimycin (final concentration: 1, 1, and 0.5 μM, respectively).

Lactate Production Assay

In fresh RPMI 1640 culture media, 1×10^6 pancreatic cancer cells (SW1990 and PDX1) were co-cultured with hCAFs (human tumor-associated fibroblasts) at a 1:1 ratio for 4 h. The concentrations of lactic acid in the supernatant were measured by a lactate assay kit.

Subcutaneous Mouse Model

The Ethics Committee of Tianjin Medical University Cancer Institute and Hospital approved all proposed animal experiments, which were conducted in accordance with NIH guidelines. The pancreatic cancer cells were utilized to establish subcutaneous xenograft in 4-6-week-old C57BL/6J mice or BALB/c-nude mice, and the mice were then randomly assigned to 6 groups. Primary murine-derived fibroblasts for MME^+ and MME^- subpopulations were sorted, mixed with murine-derived KPC cell lines, and then subcutaneously injected into immunodeficient mice. For the subcutaneous tumor model, the indicated pancreatic cancer cells at a dilution range of 1×10^6 mixed with an equal amount of CAFs were suspended in 40 μl of PBS and then subcutaneously transplanted into each mouse's flank. Related drugs were intraperitoneally injected one week later. The drug of interest was IOX2, with an IC50 of 22 nM. For the in vivo administration of IOX2 to mice, a dosage of 10 mg/kg was given via intraperitoneal injection once a week for a total of 3 weeks. For the AG regimen, 1000 mg/kg/week of gemcitabine (GEM) plus 300 mg/kg/week of Abraxane (AB) were injected intraperitoneally and administered once a week for 3 weeks. Immunotherapy involved the use of anti-PD1 (programmed cell death protein 1) antibodies, specifically the in vivo RMP1-14 antibody. The concentration of the solution was 2 mg/ml. Each mouse was intraperitoneally administered 200 μg once a week for a total of 3 weeks. The control group of IOX2 and AG were injected with the same volume of DMSO. The controls of anti-PD1 were injected with isotype IgG (Go in vivo RTK2758). The observers and recorders in the study were blinded to the grouping. Tumor growth was monitored every three days using a caliper, and tumor volumes were calculated by the following formula: Volume = 1/2 $L1 \times (L2)^2$, where L1 is the length of the long axis and L2 is the length of the short axis.

Functional Analysis

Gene ontology (GO) analysis and Kyoto Encyclopedia of Genes and Genomes (KEGG) pathway enrichment analysis were performed to determine the biological functions of the DEGs using the cluster Profiler package. GO enrichment analysis included cellular component (CC), molecular function (MF), and biological process (BP) [33]. The parameters were configured with a significance level (p-value) of less than 0.01, a minimum count threshold of 3, an enrichment factor greater than 1.5, and a statistically significant threshold of p-value less than 0.05. The Gene Set Enrichment Analysis (GSEA) was used to enrich differentially expressed mRNA pathways, and 10,000 permutations were performed for each analysis. The KEGG Pathways dataset was selected from the curated Gene Sets. The threshold for the statistically significant GSEA analysis was set to the corrected $p<0.05$ and false discovery rate (FDR) <0.25. The reference gene set chosen was "c2.cp.kegg.v7.0.symbols.gmt". A significance level of $P<0.05$ and a false discovery rate (FDR) of less than 0.25 were used to determine significant enrichment. The result of enrichment analysis would be characterized by corrected p-values and NES. GSEA enrichment analysis and visualization were performed in GSEA local software.

Statistical Analysis

Statistical analyses were performed in GraphPad Prism-6.0. The data were reported as the mean ± standard deviation (SD) unless specified otherwise. The variance between different groups was statistically compared, and $p<0.05$ was considered statistically significant. Power analysis was conducted on the results. Student's t-test was used to compare the mean values. One-way ANOVA was carried out for the analysis of mouse tumor growth. The differential gene analysis was conducted using the top Table and decide methods. The limma package provided test functions for summarizing linear model results, performing hypothesis tests, and adjusting p-values for multiple tests. The log-rank algorithm was performed to compare statistical differences in survival curves. The Pearson test was also used to conduct correlation analysis. $^*P<0.05$; $^{**}P<0.01$; $^{***}P<0.001$; $^{****}P<0.0001$ and n.s., non-significant.

Results

Single-Cell Transcriptome Analysis of Pancreatic Cancer Samples Reveals Heterogeneity of Fibroblasts

To examine the role of fibroblasts in the progression of pancreatic cancer, the proportion of fibroblasts in various pancreatic cancer patient samples was determined using cell infiltration algorithms, including XCELL, EPIC, and MCPCOUNTER. The three algorithms demonstrated a high degree of agreement (Figure S1A). The

highest scores were observed in patients with grade 3, stage III-IV, and T2-3 pancreatic cancers (Figure S1B-D), as evidenced by the comparison of cancer-related fibroblast scores in various clinical subgroups. This suggests that fibroblasts are crucial in the progression of pancreatic cancer. Survival prognostic analysis also showed that patients with highly infiltrated fibroblasts had a worse prognosis and shorter survival time (Figure S1E-F). Therefore, it is worthwhile to study the mechanism of fibroblasts in pancreatic cancer patients.

Single-cell data analysis can better reveal the heterogeneity among different cells. By annotating cellular subpopulations, subpopulations of ductal epithelial cells, T cells, B cells, macrophages, endothelial cells, and fibroblasts were identified in pancreatic cancer (Fig. 1A, Figure S2). Compared to other subpopulations, fibroblasts were significantly more frequent in patients with moderately to severely differentiated, vascular invasion, peripheral nerve infiltration, and progressive pancreatic cancer (Fig. 1A). The LUM gene was utilized to extract and down-cluster fibroblasts. Subsequently, seven distinct fibroblast subtypes were identified by annotating them with genes that were expressed at significantly different levels (Fig. 1B-D). The assessment of the cell cycle of the seven fibroblasts revealed that the MME^+ CAFs had a greater proportion of cells in the S-phase. This indicates the higher proliferative activity of this particular cell population (Fig. 1E). The results also showed that MME^+ CAFs were more prevalent in patients with moderately to severely differentiated, vascular invasion, peripheral nerve infiltration, and pancreatic cancer progression, suggesting that this type of fibroblasts plays a crucial role in the progression of pancreatic cancer (Fig. 1F).

MME^+ Fibroblasts are Associated with Multiple Cancer Pathway Activities and Promote Pancreatic Cancer Progression through the Hypoxia-Related Signaling Pathway

The differential analysis of various subtypes of fibroblasts demonstrated that each cell subpopulation exhibited distinct patterns of highly expressed genes. Notably, MME^+ CAFs showed high expression of genes such as MIF, ALODA, and GAPDH (Fig. 2A-B). Functional enrichment was conducted on these CAFs due to the heterogeneity of fibroblast subpopulations, which serve distinct functions in tumors. Pathway enrichment of different fibroblast subpopulations revealed that the MME^+ fibroblast population was associated with glucose metabolism, HIF-1 signaling pathway, and tumor-typical signaling pathways such as MYC, P53, E2F, and DNA damage repair (Fig. 2C-D). The $KDM6B^+$ fibroblast was enriched in the IL-17 signaling pathway, TNF signaling pathway, and IL-18 signaling pathway. The results indicated that the $COL11A^+$ fibroblast was mainly involved in the ECM-receptor interaction and focal adhesion; the $FBLN^+$ fibroblast was associated with pancreatic secretion; the $EMP1^+$ fibroblast was correlated with complement and coagulation cascades; and the $COL4A1^+$ fibroblast was related with tissue remodeling and inflammatory response to wounding. The $BTG1^+$fibroblast was mainly enriched in the antigen processing and presentation (Fig. 2C-D). The MME^+ cell subpopulation was compared to other subpopulations of tumor cells and immune cells. It was found that the MME^+ cells are actively involved in pathways influenced by hypoxia, such as the MIF, VEGF, TGFB, CALCR, and ANGPTL4 pathways (Fig. 2E-I). A time-series analysis of fibroblasts revealed that MME^+ fibers were at the end of the fibroblast evolutionary spectrum 1 (Fig. 3A-B). The MIF gene, which has been reported to be one of the hallmark genes of hypoxia, was also expressed in MME^+ fibroblasts in addition to MME. This suggests that the MME^+ fibroblasts were prone to forming a hypoxic TME, which in turn activated the MIF signaling pathway (Fig. 3C). The study of genes developing along the trajectory of cell differentiation indicated that hypoxia-related ADM and TGFBI played a key role in driving the formation of MME^+ fibers, further illustrating the close association between MME^+ fibroblasts and the formation of a hypoxic environment in tumors (Fig. 3D).

Genomic and Transcriptomic Analysis of Pancreatic Cancer Patients After Differential Grouping by MME^+CAF

In two combined datasets, TCGA and CPTAC, the prognostic relationship between this fibroblast score and pancreatic cancer patients was evaluated by organizing the highly expressed genes of MME^+ fibroblasts into gene sets. The results revealed the poorer prognosis of patients in the highly infiltrated MME^+ fibroblasts group (Fig. 4A). As expected, the MME^+ fibroblast score was higher in patients with high-grade and advanced-stage pancreatic cancer (Fig. 4B), suggesting that MME^+ fibroblasts play a key role in the progression and deterioration of pancreatic cancer. Genomic analysis was conducted on the high- and low-infiltration groups of MME^+ CAFs to investigate the mechanism of fibroblast production. The results indicated that the mutation rates of oncogenes, including KRAS and TP53, were slightly higher in the high-infiltration group, suggesting that mutations of typical oncogenes may facilitate the production of MME^+ fibroblasts (Fig. 4C-D). Differential analysis and GSEA analysis of the high and low infiltration groups revealed that the high infiltration group was positively enriched for the hypoxia pathway, MYC signaling pathway, EMT, and G2M checkpoint signaling pathway, while the low infiltration group was associated with downregulation of bile metabolism and KRAS activity pathway (Fig. 4E-F). Transcriptome sequencing was performed on a sample

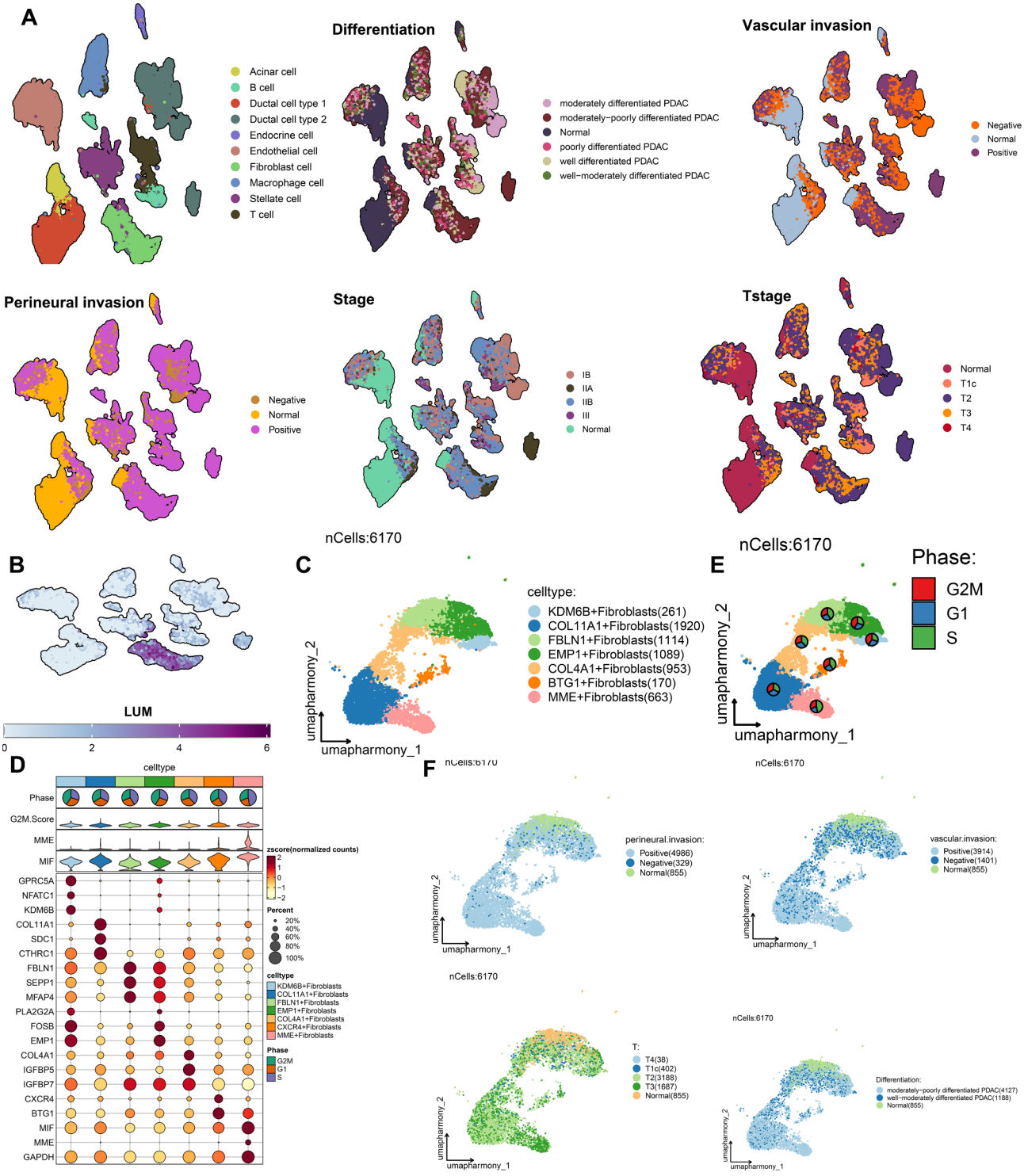

Fig. 1 Single-cell transcriptome landscape of pancreatic cancer patients. **(A)** UMAP plots of cell subpopulations with descending clustering as well as UMAP plots of cells at different levels of differentiation, vascular infiltration, peripheral nerve infiltration, staging, and T-staging. **(B)** LUM gene expression UMAP plot. **(C)** UMAP plot of fibroblast subpopulations. **(D)** Bubble plots showing typical gene expression in each fibroblast subpopulation. **(E)** Cellular staging of different fibroblast subpopulations. **(F)** UMAP downscaling plots of different fibroblast subpopulations in peripheral nerve infiltration, vascular infiltration, different T-stages, and different degrees of differentiation

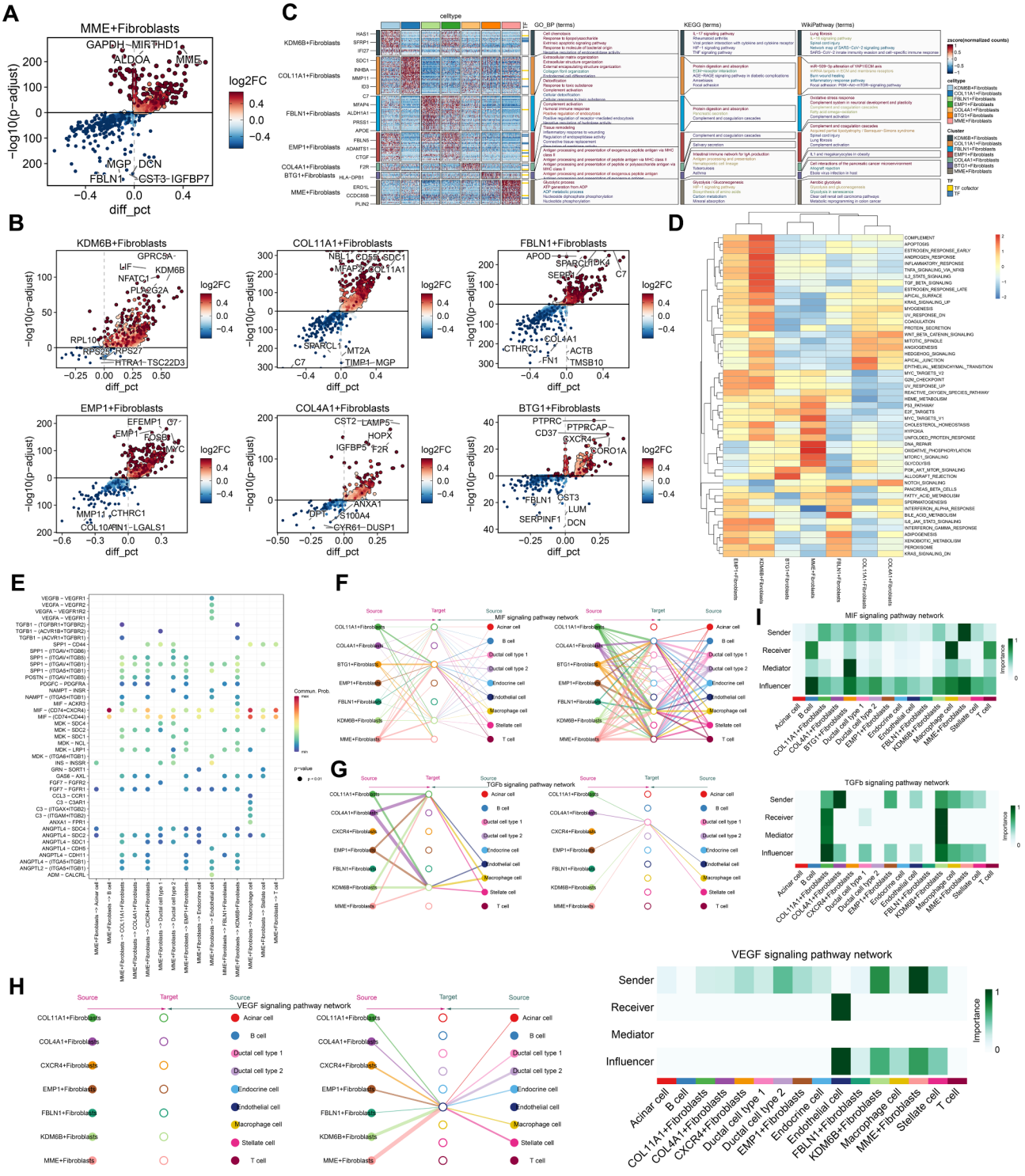

Fig. 2 Signaling pathways involved in MME $^{+}$ fibroblasts. **A-B**. Volcano plots demonstrating high and low differentially expressed genes in MME^{+} fibroblasts **(A)** and other subtypes of fibroblasts **(B). C.** Heatmap of GO, KEGG, and wiki pathway pathways enriched for highly expressed genes in different fibroblast subpopulations. **D.** Heatmap of 50 typical cancer pathway scores enriched in different fibroblast subpopulations. **E.** Bubble diagram of ligand-receptor interactions between MME^{+} fibroblasts and other cell subpopulations. **F-H.** Connection diagrams of MIF **(F)**, TGFb **(G)**, and VEGF **(H)** interactions signaling pathways in fibroblast subpopulations and other distinct cellular subpopulations. **I.** Heatmaps of the roles of different cellular subpopulations in the MIF, TGFb, and VEGF signaling pathways in the cellular communication network, including senders, receivers, mediators, and influencers

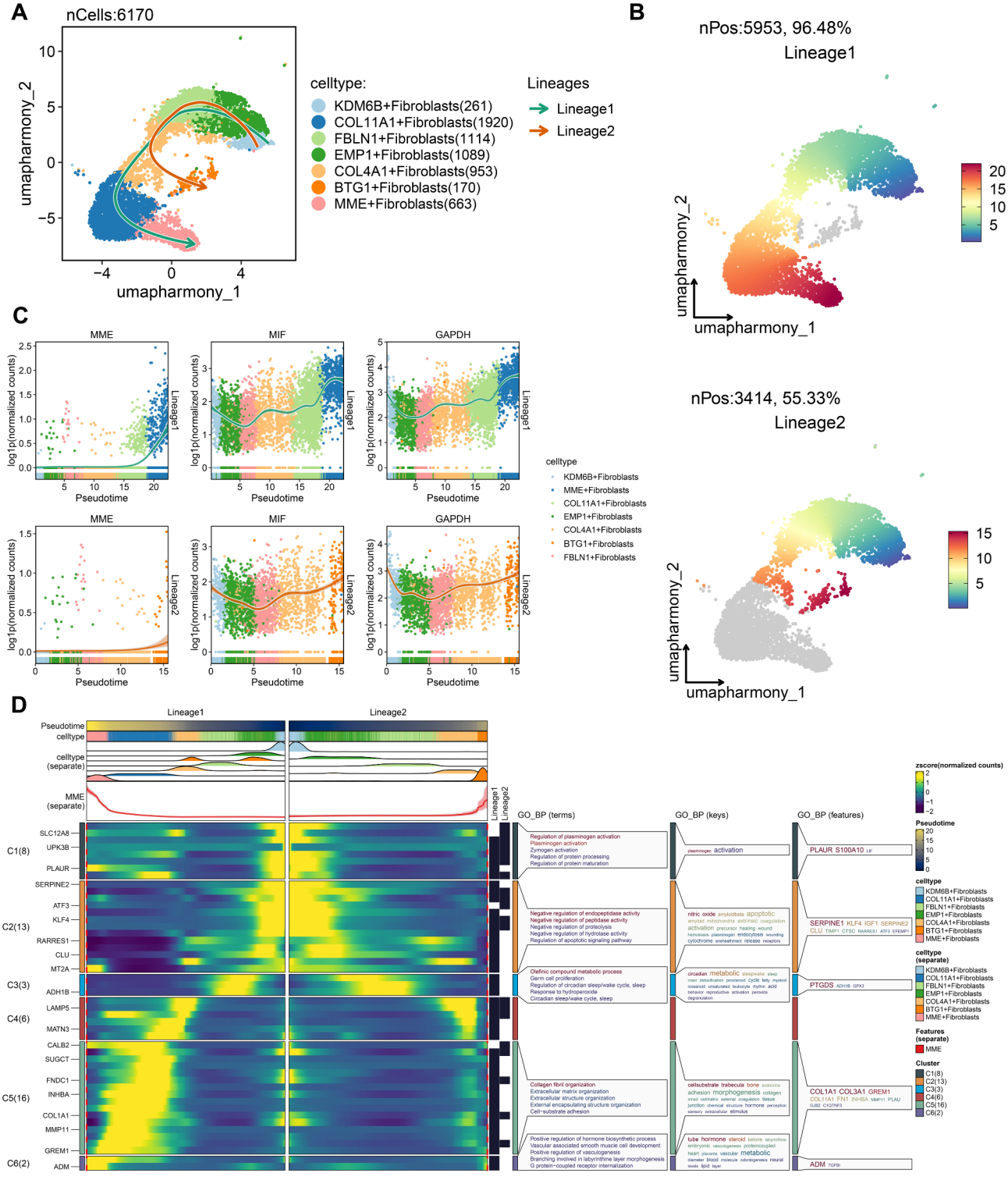

Fig. 3 Proposed temporal analysis of fibroblast subpopulations. **A.**. Cell evolutionary trajectory of the start and end points of fibroblast evolution. **B.** UMAP plots of the timing of the proposed chronology of different cellular evolutions. **C.** Expression of different genes in different fibroblast subpopulations increases or decreases with the evolutionary trajectory. **D**. Heatmap of genes that drive differentiation and development of fibroblasts along a trajectory with pathway functional enrichment

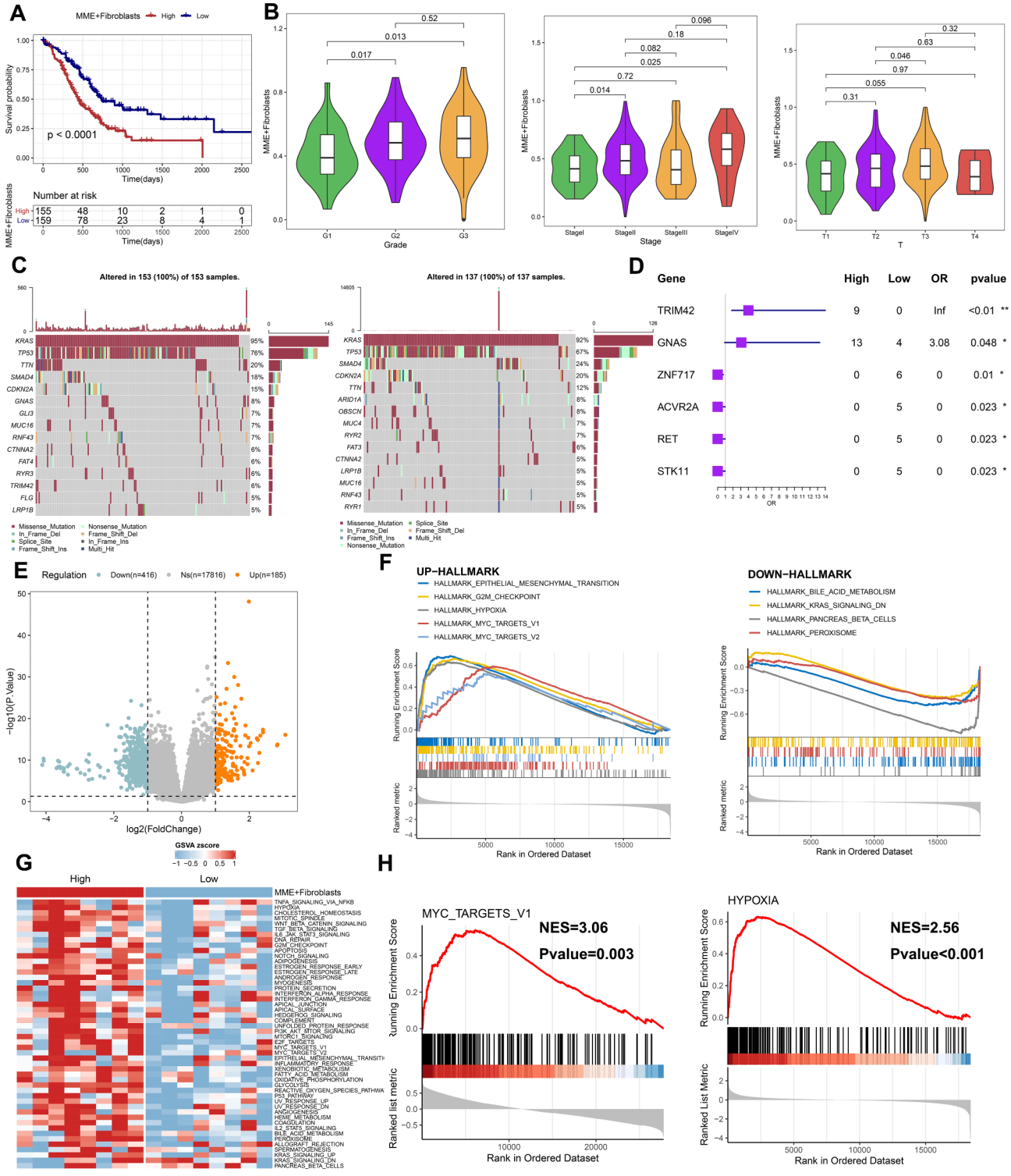

Fig. 4 Analysis of MME $^{+}$ fibroblasts in bulk multi-omics. (**A**) KM survival curves of survival differences between high and low MME^{+} fibroblast groups. **(B)** Box plots of differences in MME^{+} fibroblast scores in patients with different staging grades. **(C)** Waterfall plot of top 15 gene mutations in the high and low infiltrating MME^{+} fibroblast groups. **(D)** Forest plot of genes with significant mutational differences between the two groups. **(E)** Volcano plot of the differentially expressed genes (DEGs) in the high and low groups **(F)** GSEA plot of the pathways positively and negatively enriched in MME^{+} fibroblasts **(G)** Heatmap of differences in cancer pathway activity in the self-tested group of high- and low-infiltrating MME^{+} fibroblasts of pancreatic cancer samples **(H)** Scores of MME^{+} fibroblasts populations enriched for the MYC and hypoxia pathways

of 16 patients to verify the difference in transcriptome pathway activity in the high infiltration group. The results showed that the cancer pathway activity was elevated in the high MME$^+$ CAFs group compared with the low infiltration group (Fig. 4G). In particular, the hypoxia and MYC pathways were highly enriched in the highly infiltrated group (Fig. 4H).

Sensitivity of MME$^+$ Fibroblasts to Chemotherapeutic Agents in high and low Infiltration Groups

The GDSC database and the cell line drug sensitivity dataset were employed to analyze the treatment differences between the high and low infiltration groups to investigate the role of MME$^+$ fibroblasts in the treatment of pancreatic cancer patients (Fig. 5A). Patients in the high infiltration group exhibited resistance to chemotherapeutic agents, including platinum, cyclophosphamide, and paclitaxel. This suggests that the presence of MME$^+$ CAFs posed a significant challenge in effectively treating patients with pancreatic cancer (Fig. 5B). The top 30 genes associated with MME$^+$ CAFs were chosen for cMAP small molecule drug prediction to predict the effects of drugs on these cells. Notably, the MTOR inhibitor torin-2, the protein kinase inhibitor NVP-TAE226, and the P450 inhibitor clotrimazole were effective drugs against MME$^+$ CAFs (Fig. 5C). The BCL inhibitor TW-37, the kinase agonist PAC-1, and the PKC inhibitor sotrastaurin were potent against MME$^+$ CAFs (Fig. 5D).

MME$^+$ Fibroblasts Promote Immunosuppressive Microenvironment Formation

The immune cell infiltration assessment algorithms, such as CIBERSORT, XCELL, EPIC, and TIMER, were employed to compare MME$^+$ and MME$^-$ CAFs in the characteristics of the immune microenvironment. These algorithms help determine the role of MME$^+$ fibroblasts in mediating signal exchange and transduction in the immune microenvironment. The results showed that the highly enriched group of MME$^+$ fibroblasts was accompanied by a large infiltration of neutrophils, mast cells, Tregs, and monocyte macrophages, and a smaller infiltration of CD8+T cells, NK cells, and dendritic cells. (Fig. 6A-B). The overall immune microenvironment activation and depletion characteristics were also assessed, and the results indicated that patients enriched with MME$^+$ CAFs had a depleted and inactivated immune microenvironment (Fig. 6C). Moreover, both immune exclusivity and immune TIDE scores were more pronounced in the MME$^+$ fibroblast-enriched group (Fig. 6D-E). It suggests that MME$^+$ fibroblasts have a significant inhibitory effect on the immune microenvironment of pancreatic cancer, which may potentially influence the subsequent immunotherapy of pancreatic cancer.

MME$^+$CAFs Promote Tumor Growth by Mediating the Formation of Immunosuppressive TME and Enhancing Aerobic Glycolysis in Pancreatic Cancer Cells

The effects of MME$^+$ CAFs on the progress of pancreatic cancer were further evaluated through a series of in vivo and in vitro experiments. MME$^+$ CAFs and MME$^-$CAFs were sorted by flow cytometry from the CAFs derived from tumor tissues of pancreatic cancer patients (Fig. 7A). The expression level of MME protein in MME$^-$ CAFs and MME$^+$ CAFs was verified by Western blot (Fig. 7B). Pancreatic cancer cells (KPC) derived from mice were mixed with PBS, MME$^-$ CAFs, or MME$^+$ CAFs at a 1:1 ratio. These mixtures were then subcutaneously transplanted to C57BL/6J mice, which were randomly divided into three groups: Ctrl, MME$^-$ CAFs, and MME$^+$ CAFs. After 28 days, the tumors were collected for further analysis. MME$^+$ and MME$^-$ murine-derived primary fibroblasts were obtained from tumor tissues of KPC mice. The tumor burden of the MME$^+$ CAFs group was significantly boosted compared with the control and MME$^-$ CAFs groups (Fig. 7C-D). The results obtained from the harvested tumors showed a significant increase in the Ki67 level, which is a well-known marker for cell proliferation, in the MME$^+$CAFs group. Additionally, there was a significant decrease in the TUNEL level, which is an index for apoptosis, in the same group (Fig. 7E). The effects of MME$^+$ CAFs on the tumor immune microenvironment were also evaluated. Flow analysis results demonstrated that MME$^+$ CAFs minimized the number of CD8$^+$T cells and effector CD8$^+$T cells secreting killer proteins (TNFα, Granzyme B, and IFNγ) and increased exhausted CD8$^+$PD1$^+$T cells and Tregs (CD4$^+$CD25$^+$Foxp3$^+$ T cell) (Fig. 7F). Meanwhile, MME$^+$ CAFs also increased the proportion of tumor-infiltrated myeloid cells, which include granulocytic myeloid-derived suppressor cells (Gr-MDSCs, CD45$^+$CD11b$^+$Ly6G$^+$) and monocytic myeloid-derived suppressor cells (Mo-MDSCs, CD45$^+$CD11b$^+$Ly6C$^+$), as well as tumor-associated macrophages (CD45$^+$CD11b$^+$F4/80$^+$) (Fig. 7G). These results indicated that MME$^+$ CAFs promote the formation of tumor immunosuppression microenvironment. The above analyses suggested that MME$^+$ CAFs might participate in cellular energy metabolism. Therefore, this study also validated the role of MME$^+$ CAFs in the progress of aerobic glycolysis. Pancreatic cancer cells were co-cultured with an equivalent amount of CAFs in vitro (Fig. 7H). The results showed that MME$^+$ CAFs can promote the expression of glycolysis-related biomarkers (i.e., MCT1, MCT4, GLUT1, GLUT4, and LDHA) on the mRNA and protein level (Fig. 7I-J). In addition, MME$^+$ CAFs significantly increased the glycolysis-associated ECAR and decreased the OXPHOS-associated OCR used for ATP production (Fig. 7K-L). Similarly, MME$^+$

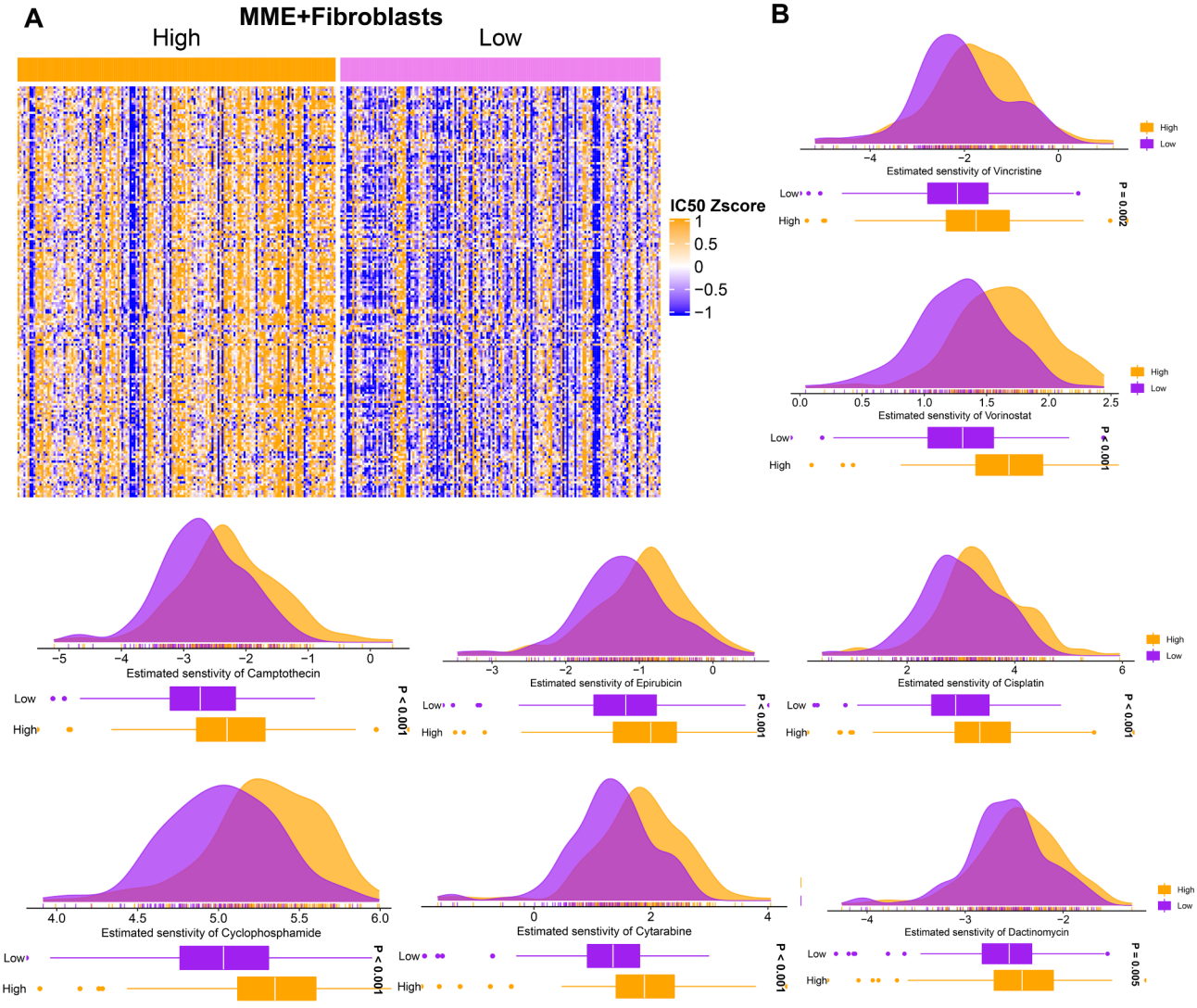

C

Drug	Mechanism	Score
torin-2	MTOR inhibitor	-0.74
NVP-TAE226	Protein tyrosine kinase inhibitor	-0.74
clotrimazole	Cytochrome P450 inhibitor	-0.72
NVP-TAE684	ALK inhibitor	-0.71
cabozantinib	VEGFR inhibitor	-0.71
HA-1004	Calcium channel blocker	-0.7
pazopanib	VEGFR inhibitor	-0.7
fluvastatin	HMGCR inhibitor	-0.69
SA-94315	Caspase inhibitor	-0.68
meisoindigo	STAT inhibitor	-0.68

D

Drug	Mechanism	Score
TW-37	BCL inhibitor	0.67
CAY-10618	NAMPT inhibitor	0.67
PAC-1	Caspase activator	0.67
sotrastaurin	PKC inhibitor	0.67
butein	EGFR inhibitor	0.69
ciclopirox	Membrane integrity inhibitor	0.69
DMH1	ALK inhibitor	0.7
LY-2811376	Beta secretase inhibitor	0.7
MLN-4924	Nedd activating enzyme inhibitor	0.7
chloroxine	Opioid receptor antagonist	0.71

Fig. 5 Chemotherapeutic agents predicted to target MME $^{+}$ fibroblasts. **(A)** Heatmap of the sensitivity of high and low MME^{+} fibroblasts to chemotherapeutic agents (IC50 values). **(B)** Boxplots and densitograms jointly show the sensitivity of high and low MME^{+} fibroblast groups to specific drugs **C-D.** The CMap database predicts effective chemotherapeutic drugs based on positively and negatively correlated genes in MME^{+} fibroblasts, where a smaller score represents more effective treatment for MME^{+} fibroblasts **(C)**, and a larger score represents that the drug is positively correlated with MME^{+} fibroblast scores and is not effective for treatment **(D)**

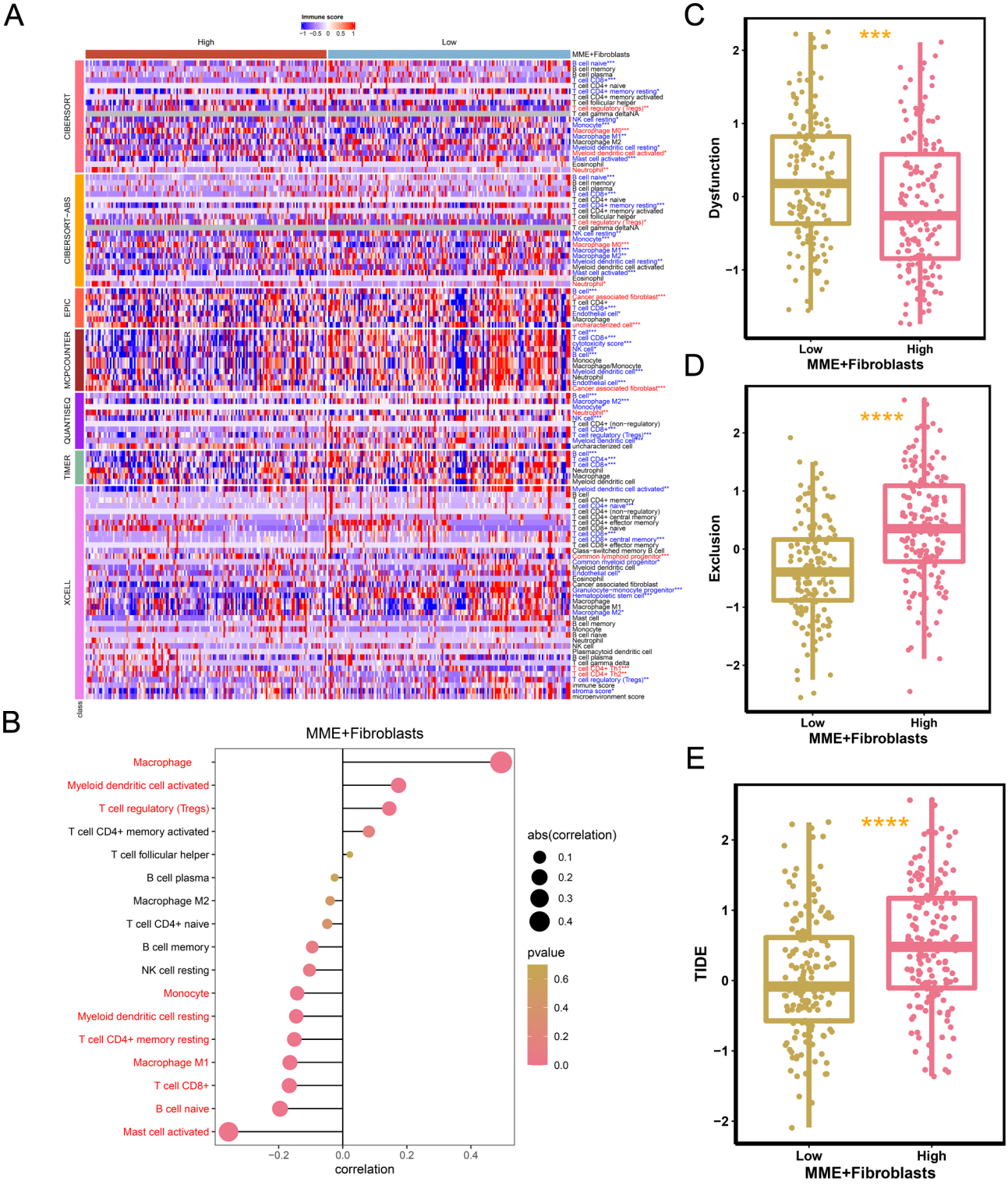

Fig. 6 Assessment of the immune microenvironment of MME $^{+}$ fibroblasts. **A.** The differences between the MME^{+} and MME^{-} fibroblast groups in the immune microenvironment and infiltration characteristics were assessed using immune infiltration algorithms such as CIBERSORT, XCELL, EPIC, and TIMER; **B.** The correlation between MME^{+} fibroblasts and immune cells in the immune microenvironment was calculated and shown in a bar graph; **C.** The functional scores of the MME^{+} and MME^{-} fibroblast groups were compared; **D.** Calculating the immune exclusivity between the MME^{+} and MME^{-} fibroblast groups; **E.** Calculating the functional TIDE scores for the MME^{+} and MME^{-} fibroblast groups

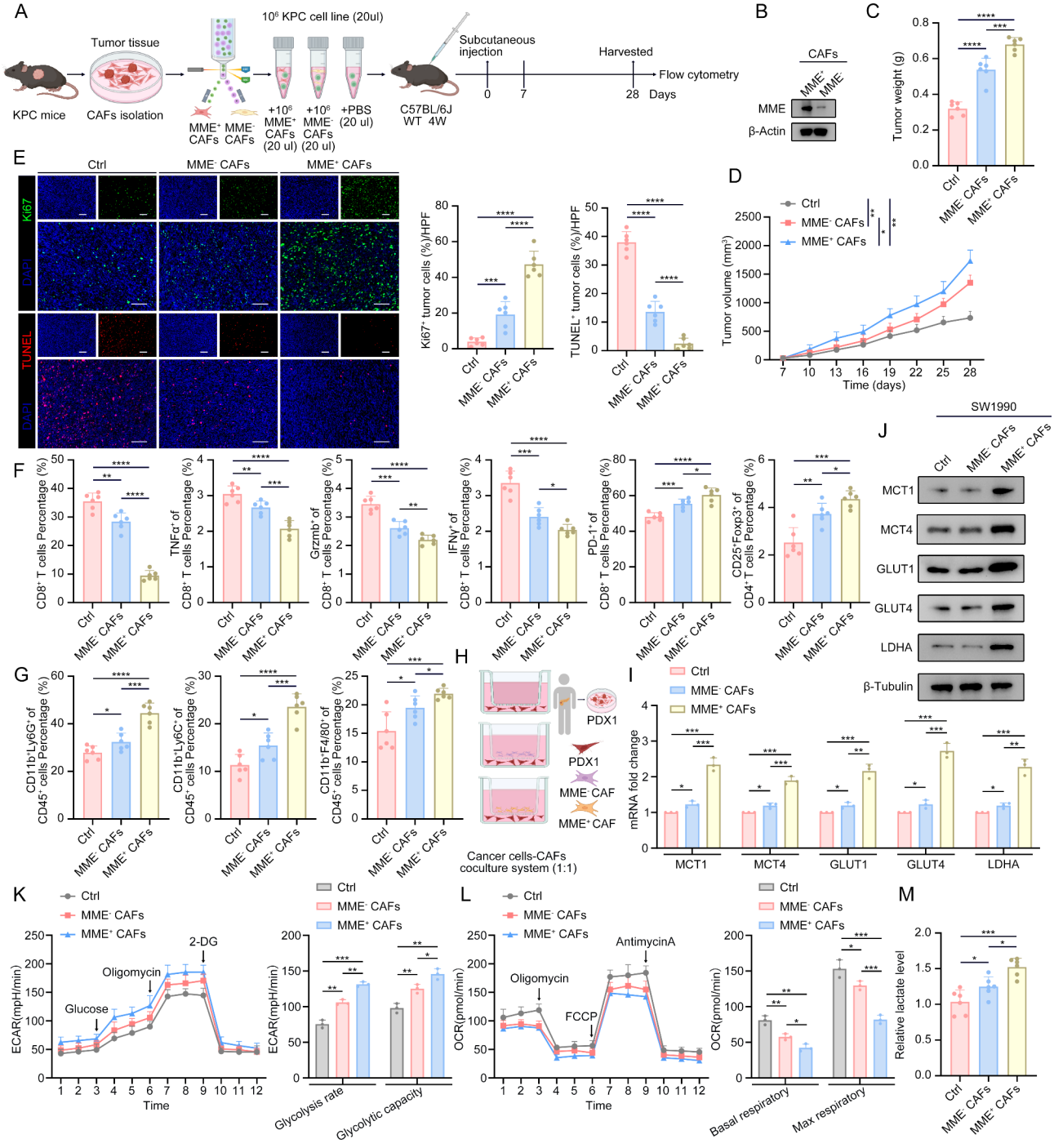

Fig. 7 (See legend on next page.)

CAFs also enhanced lactate production in pancreatic cancer cells (Fig. 7M).

Additionally, lentiviruses that stably overexpress the MME protein were developed and assembled. They were then transfected into mCAF cell lines and combined with murine-derived KPC cell lines for subcutaneous injection into C57BL/6J mice (Figure S3 A-B). The results showed that the MME-overexpressing CAFs promoted tumor growth and proliferation (Figure S3C-E), and enhanced the formation of immunosuppressive TME. This consisted of a decreased number of CD8+T cells and their functional biomarker, as well as an increased presence of exhausted T cells, tumor-infiltrating Tregs, and myeloid cells (Figure S3F-G). In vitro experiments demonstrated that the MME-overexpressing CAFs promoted the progress of aerobic glycolysis in pancreatic cancer cells

(See figure on previous page.)

Fig. 7 MME $^{+}$ CAFs promote tumor growth by mediating the formation of immunosuppressive TME and enhancing aerobic glycolysis in pancreatic cancer cells. **(A)** A schematic view of the in vivo experimental design. MME + and MME- mCAFs were extracted from the tumor tissues of KPC mice and injected subcutaneously into C57BL/6J mice in a mixture with murine-derived KPC cell lines. **(B)** The expression level of MME in MME^{-} CAFs and MME^{+} CAFs groups was measured by Western blot. **(C)** Tumor weight was analyzed when the tumors were harvested 28 days after the subcutaneous implantation. **(D)** The growth curve was plotted according to the size of the tumor once every three days. **(E)** Immunofluorescence staining was performed on the subcutaneous tumor of each group using Ki67 and TUNEL, and the representative images were shown. The development of multiplex fluorescent IHC was primarily conducted following the formation of subcutaneous tumors by injecting a mixture of mouse-derived CAF and mouse-derived KPC cell lines for sectioning. The Ki67^{+} and TUNEL^{+} tumor cells were analyzed in Image-J. **(F)** Percentage of tumor-infiltrated CD8^{+} T-cells and related functional markers (TNFα, Grzmb, IFNγ, and PD1) and Tregs was determined in each group by flow cytometry. **(G)** Percentage of tumor-infiltrated myeloid cells in each group was determined by flow cytometry. **(H)** A schematic view of the cancer cells-CAFs coculture system. Human-derived CAFs were co-cultured with the pancreatic cancer cell line (Pancreatic cancer primary cell lines, PDX1). **(I)** The expression level of glycolysis-related biomarkers was measured in each group by qPCR. **(J)** The expression level of glycolysis-related biomarkers was measured in each group by Western blot. **K.** The groups were compared in terms of ECARs, and glycolysis rates and glycolytic capacity were analyzed. **L.** The groups were compared in terms of OCRs, and basal respiratory and max respiratory levels were analyzed. **M.** The relative lactate production level was examined in each group. All experiments were repeated six times independently. Unpaired Student's t-test was used for statistical analysis. *$P < 0.05$, **$P < 0.01$, ***$P < 0.001$, ****$P < 0.0001$. CAFs; Ctrl, control; Tregs, regulatory T cells; Grzmb, Granzyme B

(Figure S3 H-M). All these findings are consistent with previous results of sorting MME^{+} CAFs.

IOX2 Inhibitor Sensitizes the Pancreatic Cancer Treatment Effectiveness of AG Chemotherapy and Anti-PD1 Immunotherapy in the Presence of MME $^{+}$ CAFs

Murine-derived pancreatic cancer cells (KPC cell lines) mixed with CAFs sorted from tumor tissues of KPC mice or PBS at the ratio of 1:1 were subcutaneously transplanted into BALB/c-nude mice, which were randomly assigned to four groups: MME^{-} CAFs-AG, MME^{-} CAFs-AG+IOX2 inhibitor, MME^{+} CAFs-AG, MME^{+} CAFs-AG+IOX2 inhibitor. AG or a combination of AG and A inhibitors was administered once weekly beginning on the seventh day. The tumors were harvested 28 days after transplantation (Fig. 8A). Based on the study findings, the synergistic effect of IOX2 and AG was investigated in Synergyfinder-2.0. The comprehensive synergy scores of IOX2 with AG (26.173) indicated that IOX2 and AG exhibited synergistic lethal effects at the studied doses. (Fig. 8B). The combination of AG and IOX2 significantly inhibited the tumor growth in the MME^{+} CAFs group, when compared to the administration of the AG regimen alone; however, the AG-IOX2 inhibitor combination therapy could not significantly affect the MME^{-} CAFs group (Fig. 8C-D). To further acknowledge whether IOX2 inhibitor could alleviate tumor burden and improve the therapeutic efficacy of immunotherapy, murine-derived pancreatic cancer cells (KPC cell lines) mixed with CAFs sorted from tumor tissues of KPC mice or PBS at the ratio of 1:1 were subcutaneously transplanted into C57BL/6J mice, which were randomly assigned to four groups: MME^{-} CAFs-Anti-PD1, MME^{-} CAFs- Anti-PD1+IOX2 inhibitor, MME^{+} CAFs- Anti-PD1, and MME^{+} CAFs- Anti-PD1+IOX2 inhibitor; Anti-PD1 or a combination of Anti-PD1 and IOX2 inhibitor was administered once weekly beginning on the seventh day. The tumors were harvested 28 days after transplantation (Fig. 8E). The results indicated a robust synergy between the IOX2 inhibitor and Anti-PD1, as indicated by a ZIP Synergy score of 32.262 (Fig. 8F). The results also showed that the combination of Anti-PD1 and IOX2 decreased tumor burden more significantly than Anti-PD1 in the presence of MME^{+} CAFs (Fig. 8G-H).

Discussion

Pancreatic cancer is widely recognized for its aggressive nature and unfavorable prognosis. The TME plays a critical role in the progression of this disease [4, 48]. Among the various components of the TME, CAFs have been identified as key players [49]. CAFs are important constituents of the stromal region in pancreatic tumors that significantly affect the disease progression and therapeutic outcomes through various mechanisms [50, 51].

CAFs facilitate the development of chemo-resistant phenotypes by cultivating a niche that supports tumor growth, invasion, and metastasis, thereby circumventing the cytotoxic effects of chemotherapy [52]. They establish a protective barrier that protects malignant tumor cells from the cytotoxic effects of chemotherapeutic agents by modulating signaling pathways, promoting extracellular matrix remodeling, and granting metabolic adaptability to pancreatic cancer cells [50, 53]. The emergence of chemoresistance poses a significant obstacle to the successful treatment of pancreatic cancer, underscoring the need to gain a deeper understanding of the complex interactions between CAFs and molecular pathways involved in drug responses [47, 54]. The convergence of CAF-driven tumorigenic signals and immune evasion mechanisms highlights the importance of comprehending the dynamic interplay of these factors in shaping the pancreatic cancer microenvironment [55, 56]. Unveiling the intricacies of CAF-mediated immunosuppression is crucial for designing innovative therapeutic approaches that target both the stromal and immune components, offering new avenues for intervening in this challenging disease [57]. The exploration of the intricate relationship between CAFs and the immunosuppressive microenvironment in

pancreatic cancer aims to reveal the underlying mechanisms that drive disease progression and treatment resistance. The dissection of the molecular basis of this symbiotic interaction is an attempt to identify novel targets and combination strategies that hold promise for disrupting tumorigenic pathways, overcoming immune suppression, and improving the prognosis of pancreatic cancer patients.

The study findings suggested that the highly expressed CAFs were identified as MME$^+$CAFs through single-cell transcriptome sequencing, which was based on MME gene expression. The study further investigated the key molecular functions of high MME expression in fibroblasts, particularly its critical role in the pancreatic cancer microenvironment and its effect on tumor progression. MME gene, also known as Neprilysin, CD10, or Neutral Endopeptidase, encodes for enkephalinase [39, 40]. This transmembrane metalloprotease is widely expressed in various tissues and organs including the brain, kidney, heart, liver, etc. Its molecular structure is composed of an extracellular N-terminus, transmembrane region, and cytoplasmic C-terminus. It is involved in the degradation of neurotransmitters, metabolic regulation (e.g., hormone concentration regulation), and immune response. Moreover, it is of significant importance in the development of drugs, the study of diseases (e.g., Alzheimer's disease, hypertension, and cancer), neuroscience, and cancer research [40–43]. CD10$^+$GPR77$^+$ CAFs promote breast tumor formation and chemoresistance by providing a survival niche for cancer stem cells (CSCs) [47]. CD10+stroma signatures play a significant role in distinguishing between in situ and invasive breast cancer, as well as in predicting the prognosis of HER2(+) breast cancer patients. Additionally, these signatures may also have the potential to indicate nonresponse to chemotherapy in certain patients [58]. The CD10 expression in tumors is associated with more aggressive histologic types and increased mitotic activity, and also serves as an independent prognostic factor for patients diagnosed with malignant pleural mesothelioma [59].

This study showed that MME$^+$CAFs were in the final stage of CAF differentiation function, indicating their distinct roles in the microenvironment of pancreatic cancer. Cell communication analysis indicated that MME$^+$CAFs were more likely to participate in the hypoxia downstream signaling pathway and microenvironmental crosstalk, which might be the potential key mechanisms influencing pancreatic cancer progression. Hypoxia can cause the upregulation of MIF, VEGF, ADM, ANGPTL4, and other genes, and the activation of their signaling pathways, which further affects the progression of pancreatic cancer [60]. MIF is a hypoxia-related pleiotropic cytokine that spatially co-localizes with HIF1A [61]. VEGF and ADM are associated with neovascularization, and their high expression can be induced in a hypoxic environment [62]. ANGPTL4 is significantly upregulated in hypoxic tumor cells, causing tumor therapy resistance [63].

This study also revealed that pancreatic cancer patients with high MME expression exhibit elevated levels of metabolic pathways (MYC and glycolysis) and microenvironmental hypoxia markers (VEGF), along with significant involvement in pro-carcinogenic inflammatory signaling pathways [64]. Patients with high levels of MME$^+$CAF experienced lower overall and recurrence-free survival rates. Additionally, a significant proportion of MME$^+$CAF was associated with more advanced pancreatic cancer staging and clinical grading. These findings further underscore the role of MME$^+$CAF in the malignant transformation of the pancreatic cancer microenvironment and its significance in disease progression. CAFs in pancreatic cancer and their associated MYC signaling pathways have been identified as crucial factors promoting the disease development [65]. Additionally, the activation of the glycolysis pathway by CAFs may induce the overexpression of MYC, which may drive the proliferation and survival of tumor cells [66].

Further investigations indicated that a high proportion of MME$^+$CAF leads to immune microenvironmental imbalance and dysfunction in pancreatic cancer, promoting increased infiltration of immunosuppressive myeloid cells, Tregs, and neutrophils, among others, while inhibiting NK cells and functional cytotoxic T-cell infiltration. This further demonstrates the role of MME$^+$CAF in the malignant transformation of the pancreatic cancer microenvironment and its effect on the disease progression. Animal studies have confirmed that the high expression of MME$^+$CAF significantly increases tumor burden in PDAC. In addition, the high expression of MME in CAF markedly enhances the resistance of tumor cells caused by pancreatic cancer to chemotherapy and immunotherapy. The drug sensitivity experiments and high-throughput drug screening in this study also discovered an inhibitor called IOX2, which specifically targets MME$^+$CAF. Based on in vitro experiments, IOX2 exhibited an IC50 of 25.4 μm for human tumor tissue-derived CAFs and 41.7 μm for the SW1990 cell line. Animal studies have demonstrated that the combination of IOX2 with AG and anti-PD1 effectively reduces tumor burden in pancreatic cancer, providing an efficient translational strategy targeting MME molecules in CAFs for pancreatic cancer treatment.

The study findings generally suggest that MME$^+$CAF plays a pivotal role in the pancreatic cancer microenvironment, exerting profound effects on tumor development and therapeutic response. However, our study has some limitations, we didn't have enough research about the effects of highly expressed MME on

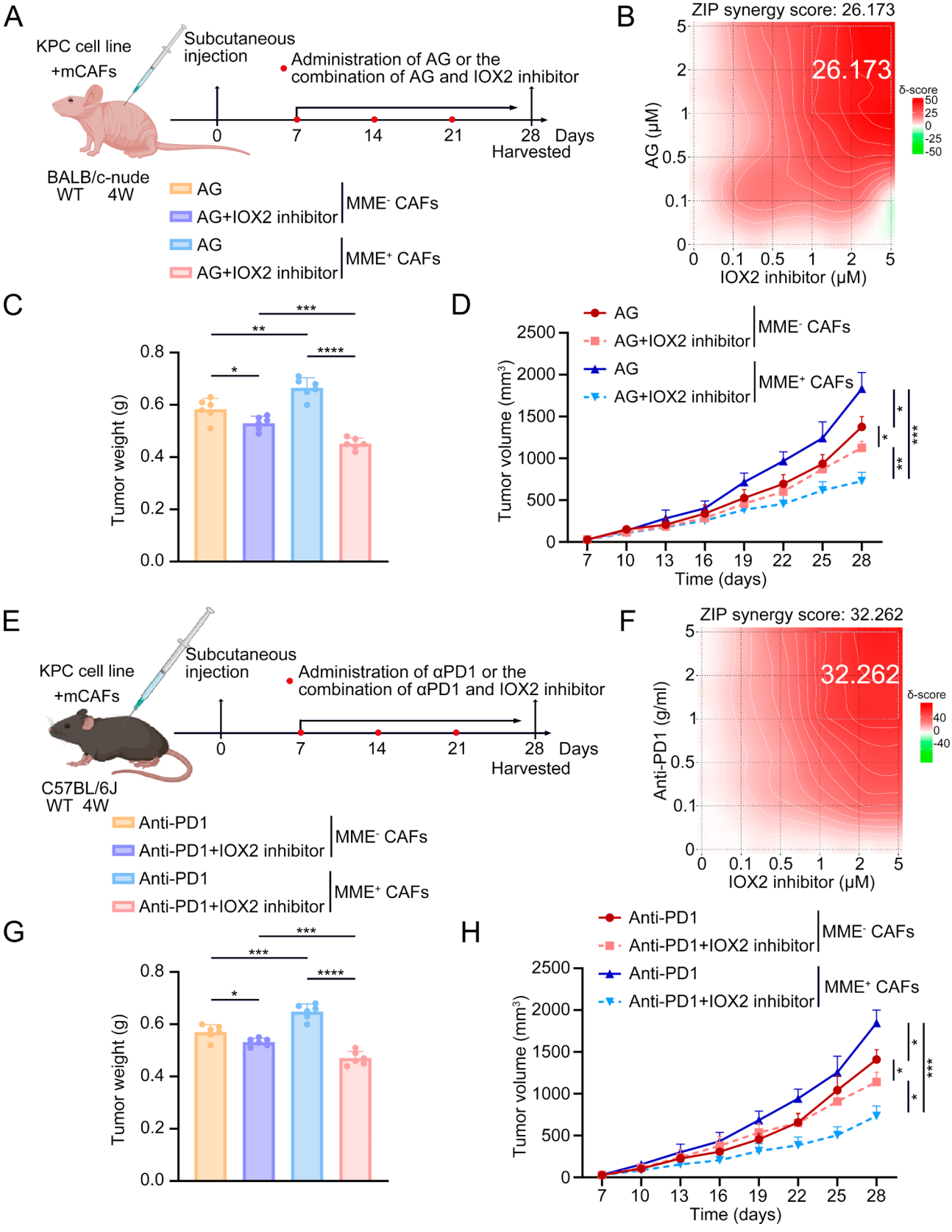

Fig. 8 (See legend on next page.)

(See figure on previous page.)

Fig. 8 IOX2 inhibitor sensitizes the pancreatic cancer treatment effectiveness of AG chemotherapy and anti-PD1 immunotherapy in the presence of MME$^+$ CAFs. **(A)** A schematic view of the experimental design. MME$^+$ and MME$^-$ mCAFs were extracted from the tumor tissues of KPC mice and injected subcutaneously into BALB/c-nude mice in a mixture with murine-derived KPC cell lines. **(B)** The functional synergistic effects of AG and IOX2 on PDAC were determined. AG, 0–5μM; IOX2 inhibitor, 0–5μM. The synergy scores of AG and IOX2 were analyzed in SynergyFinder. The AG regimen was gemcitabine combined with albumin-paclitaxel (Abraxane) at a ratio of 10:1. The AG concentration obtained in this study corresponds to the concentration of gemcitabine. **(C)** Tumor weight was analyzed when the tumors were harvested 28 days after the subcutaneous implantation. **(D)** The growth curve was plotted according to the size of the tumor once every three days. **(E)** A schematic view of the experimental design. MME$^+$ and MME$^-$ mCAFs were extracted from the tumor tissues of KPC mice and injected subcutaneously into C57BL/6J mice in a mixture with murine-derived KPC cell lines. **(F)** The functional synergistic effects of Anti-PD1 and IOX2 on PDAC were determined. Anti-PD1, 0–5μM; IOX2 inhibitor, 0–5μM. The apoptotic rate of tumor cells co-cultured with PBMCs was detected by flow cytometry and analyzed in SynergyFinder. **(G)** Tumor weight was analyzed when the tumors were harvested 28 days after the subcutaneous implantation. **(H)** The growth curve was plotted according to the size of the tumor once every three days. All experiments were repeated six times independently. Unpaired Student's t-test was used for statistical analysis. $^*P<0.05$, $^{**}P<0.01$, $^{***}P<0.001$, $^{****}P<0.0001$. CAFs

immunosuppressive gene expression at the transcriptional level, post-translational level, or related kinase activity. Future studies can further validate the biological functions of MME$^+$CAF, explore potential intervention strategies, and consider assessing the value of MME$^+$CAF as a prognostic factor in clinical practice.

Supplementary Information

The online version contains supplementary material available at https://doi.org/10.1186/s12575-024-00254-1.

Supplementary Material 1

Supplementary Material 2

Supplementary Material 3

Supplementary Material 4

Supplementary Material 5

Supplementary Material 6

Supplementary Material 7

Acknowledgements
Not applicable.

Author Contributions
B.W.,Y.P. and Y.X. wrote original draft and operated experiments. Y.Y. and H.S. investigated data. Z.Y. provided conceptions. Y.C. and L.L. edited the final version of draft. Y.Z. Performed bioinformatic analysis. W.L. and Z.P. projected administration and funding acquisition. All authors reviewed the manuscript.

Funding
This work was supported by grants from Tianjin Key Medical Discipline (Specialty) Construction Project (TJYXZDXK-009 A); Tianjin Health Research Project (TJWJ2023QN012); National Natural Science Foundation of China (82303718).

Data Availability
No datasets were generated or analysed during the current study.

Declarations

Ethics Approval and Consent to Participate
The Cancer Institute of Tianjin Medical University and the Hospital Ethics Committee (bc20240074) approved the use of all samples and participants' information. Animal procedures were performed in accordance with the Ethics Committee of the Tianjin Medical University Cancer Institute and Hospital.

Consent for Publication
The authors declare their agreement for publication.

Competing Interests
The authors declare no competing interests.

Author details
[1]Tianjin's Clinical Research Center for Cancer, Tianjin Key Laboratory of Digestive Cancer, Department of Integrative Oncology, Key Laboratory of Cancer Prevention and Therapy, Tianjin Medical University Cancer Institute & Hospital, National Clinical Research Center for Cancer, Tianjin 300060, China
[2]Department of Acupuncture and Moxibustion, First Teaching Hospital of Tianjin, University of Traditional Chinese Medicine, National Clinical Research Center for Chinese Medicine Acupuncture and Moxibustion, Tianjin 300193, China
[3]Tianjin's Clinical Research Center for Cancer, Tianjin Key Laboratory of Digestive Cancer, Department of Pancreatic Cancer, Key Laboratory of Cancer Prevention and Therapy, Tianjin Medical University Cancer Institute & Hospital, National Clinical Research Center for Cancer, Tianjin 300060, China
[4]Tianjin's Clinical Research Center for Cancer, Tianjin Key Laboratory of Digestive Cancer, Department of Pain Management, Key Laboratory of Cancer Prevention and Therapy, Tianjin Medical University Cancer Institute & Hospital, National Clinical Research Center for Cancer, Tianjin 300060, China
[5]Tianjin's Clinical Research Center for Cancer, Key Laboratory of Cancer Prevention and Therapy, Tianjin Medical University Cancer Institute & Hospital, National Clinical Research Center for Cancer, Tianjin 300060, China

Received: 17 June 2024 / Accepted: 4 September 2024
Published online: 28 September 2024

References

1. Mizrahi JD, et al. Pancreatic cancer. Lancet. 2020;395(10242):2008–20.
2. Klein AP. Pancreatic cancer epidemiology: understanding the role of lifestyle and inherited risk factors. Nat Rev Gastroenterol Hepatol. 2021;18(7):493–502.
3. Halbrook CJ, et al. Pancreatic cancer: advances and challenges. Cell. 2023;186(8):1729–54.
4. Ho WJ, et al. The tumour microenvironment in pancreatic cancer - clinical challenges and opportunities. Nat Rev Clin Oncol. 2020;17(9):527–40.
5. Sherman MH, et al. Tumor Microenvironment in Pancreatic Cancer Pathogenesis and Therapeutic Resistance. Annu Rev Pathol. 2023;18:123–48.
6. Park W, et al. Pancreat Cancer: Rev Jama. 2021;326(9):851–62.
7. Vincent A, et al. Pancreatic cancer. Lancet. 2011;378(9791):607–20.
8. Zhang H, et al. Define cancer-associated fibroblasts (CAFs) in the tumor microenvironment: new opportunities in cancer immunotherapy and advances in clinical trials. Mol Cancer. 2023;22(1):159.
9. Biffi G, et al. Diversity and Biology of Cancer-Associated fibroblasts. Physiol Rev. 2021;101(1):147–76.
10. Elyada E, et al. Cross-species single-cell analysis of pancreatic ductal adenocarcinoma reveals Antigen-Presenting Cancer-Associated fibroblasts. Cancer Discov. 2019;9(8):1102–23.

11. Hosein AN, et al. Pancreatic cancer stroma: an update on therapeutic targeting strategies. Nat Rev Gastroenterol Hepatol. 2020;17(8):487–505.
12. Huang H, et al. Mesothelial cell-derived antigen-presenting cancer-associated fibroblasts induce expansion of regulatory T cells in pancreatic cancer. Cancer Cell. 2022;40(6):656–e737.
13. Biffi G, et al. IL1-Induced JAK/STAT signaling is antagonized by TGFβ to shape CAF heterogeneity in pancreatic ductal adenocarcinoma. Cancer Discov. 2019;9(2):282–301.
14. Mucciolo G, et al. EGFR-activated myofibroblasts promote metastasis of pancreatic cancer. Cancer Cell. 2024;42(1):101–e1811.
15. Hou Y, et al. YTHDC1-mediated augmentation of miR-30d in repressing pancreatic tumorigenesis via attenuation of RUNX1-induced transcriptional activation of Warburg effect. Cell Death Differ. 2021;28(11):3105–24.
16. Chen M, et al. NUSAP1-LDHA-Glycolysis-lactate feedforward loop promotes Warburg effect and metastasis in pancreatic ductal adenocarcinoma. Cancer Lett. 2023;567:216285.
17. Guo D, et al. Aerobic glycolysis promotes tumor immune evasion by hexokinase2-mediated phosphorylation of IκBα. Cell Metab. 2022;34(9):1312–e246.
18. Li Z, et al. Metabolic reprogramming of cancer-associated fibroblasts and its effect on cancer cell reprogramming. Theranostics. 2021;11(17):8322–36.
19. Zang S, et al. Metabolic reprogramming by dual-targeting biomimetic nanoparticles for enhanced tumor chemo-immunotherapy. Acta Biomater. 2022;148:181–93.
20. Curtis M, et al. Fibroblasts mobilize Tumor Cell glycogen to promote proliferation and metastasis. Cell Metab. 2019;29(1):141–e559.
21. Hu Q, et al. UHRF1 promotes aerobic glycolysis and proliferation via suppression of SIRT4 in pancreatic cancer. Cancer Lett. 2019;452:226–36.
22. Becker LM, et al. Epigenetic reprogramming of Cancer-Associated fibroblasts deregulates glucose metabolism and facilitates progression of breast Cancer. Cell Rep. 2020;31(9):107701.
23. Yoshida GJ. Metabolic reprogramming: the emerging concept and associated therapeutic strategies. J Experimental Clin cancer Research: CR. 2015;34:111.
24. Hu X, et al. Shikonin reverses cancer-associated fibroblast-induced gemcitabine resistance in pancreatic cancer cells by suppressing monocarboxylate transporter 4-mediated reverse Warburg effect. Phytomedicine. 2024;123:155214.
25. Kitamura F et al. Cancer-associated fibroblasts reuse cancer-derived lactate to maintain a fibrotic and immunosuppressive microenvironment in pancreatic cancer. JCI Insight. 2023;8(20).
26. Falcomatà C, et al. Context-specific determinants of the immunosuppressive Tumor Microenvironment in Pancreatic Cancer. Cancer Discov. 2023;13(2):278–97.
27. Zhang Y, et al. Regulatory T-cell depletion alters the Tumor Microenvironment and accelerates pancreatic carcinogenesis. Cancer Discov. 2020;10(3):422–39.
28. Pushalkar S, et al. The pancreatic Cancer Microbiome promotes oncogenesis by induction of Innate and Adaptive Immune suppression. Cancer Discov. 2018;8(4):403–16.
29. Lin Y, et al. CAFs shape myeloid-derived suppressor cells to promote stemness of intrahepatic cholangiocarcinoma through 5-lipoxygenase. Hepatology. 2022;75(1):28–42.
30. Piper M, et al. Simultaneous targeting of PD-1 and IL-2Rβγ with radiation therapy inhibits pancreatic cancer growth and metastasis. Cancer Cell. 2023;41(5):950–e696.
31. Mao X, et al. Crosstalk between cancer-associated fibroblasts and immune cells in the tumor microenvironment: new findings and future perspectives. Mol Cancer. 2021;20(1):131.
32. Luong T, et al. Fibroblast heterogeneity in pancreatic ductal adenocarcinoma: perspectives in immunotherapy. Cytokine Growth Factor Rev. 2022;68:107–15.
33. Kumagai S, et al. Lactic acid promotes PD-1 expression in regulatory T cells in highly glycolytic tumor microenvironments. Cancer Cell. 2022;40(2):201–. – 18.e9.
34. Wu S, et al. Hyperglycemia enhances immunosuppression and aerobic glycolysis of pancreatic Cancer through Upregulating Bmi1-UPF1-HK2 pathway. Cell Mol Gastroenterol Hepatol. 2022;14(5):1146–65.
35. Sun F, et al. Regulating glucose metabolism with Prodrug nanoparticles for promoting photoimmunotherapy of pancreatic Cancer. Adv Sci (Weinh). 2021;8(4):2002746.
36. Zhu GQ, et al. CD36(+) cancer-associated fibroblasts provide immunosuppressive microenvironment for hepatocellular carcinoma via secretion of macrophage migration inhibitory factor. Cell Discov. 2023;9(1):25.
37. Wang Y, et al. Single-cell analysis of pancreatic ductal adenocarcinoma identifies a novel fibroblast subtype associated with poor prognosis but better immunotherapy response. Cell Discov. 2021;7(1):36.
38. Broz MT, et al. Metabolic targeting of cancer associated fibroblasts overcomes T-cell exclusion and chemoresistance in soft-tissue sarcomas. Nat Commun. 2024;15(1):2498.
39. Li M, et al. Membrane metalloendopeptidase (MME) suppresses metastasis of esophageal squamous cell carcinoma (ESCC) by inhibiting FAK-RhoA Signaling Axis. Am J Pathol. 2019;189(7):1462–72.
40. Bayes-Genis A, et al. A test in Context: Neprilysin: function, inhibition, and Biomarker. J Am Coll Cardiol. 2016;68(6):639–53.
41. Kim E, et al. Irisin reduces amyloid-β by inducing the release of neprilysin from astrocytes following downregulation of ERK-STAT3 signaling. Neuron. 2023;111(22):3619–e338.
42. D'Elia E, et al. Neprilysin inhibition in heart failure: mechanisms and substrates beyond modulating natriuretic peptides. Eur J Heart Fail. 2017;19(6):710–7.
43. Esser N, et al. Neprilysin inhibition: a new therapeutic option for type 2 diabetes? Diabetologia. 2019;62(7):1113–22.
44. Cords L, et al. Cancer-associated fibroblast classification in single-cell and spatial proteomics data. Nat Commun. 2023;14(1):4294.
45. Cords L, et al. Cancer-associated fibroblast phenotypes are associated with patient outcome in non-small cell lung cancer. Cancer Cell. 2024;42(3):396–e4125.
46. Mayakonda A, et al. Maftools: efficient and comprehensive analysis of somatic variants in cancer. Genome Res. 2018;28(11):1747–56.
47. Su S, et al. CD10(+)GPR77(+) Cancer-Associated fibroblasts promote Cancer formation and chemoresistance by sustaining Cancer Stemness. Cell. 2018;172(4):841–e5616.
48. Raghavan S, et al. Microenvironment drives cell state, plasticity, and drug response in pancreatic cancer. Cell. 2021;184(25):6119–e3726.
49. Sahai E, et al. A framework for advancing our understanding of cancer-associated fibroblasts. Nat Rev Cancer. 2020;20(3):174–86.
50. Qi R, et al. Cancer-associated fibroblasts suppress ferroptosis and induce gemcitabine resistance in pancreatic cancer cells by secreting exosome-derived ACSL4-targeting miRNAs. Drug Resist Updat. 2023;68:100960.
51. Öhlund D, et al. Distinct populations of inflammatory fibroblasts and myofibroblasts in pancreatic cancer. J Exp Med. 2017;214(3):579–96.
52. Hu C, et al. circFARP1 enables cancer-associated fibroblasts to promote gemcitabine resistance in pancreatic cancer via the LIF/STAT3 axis. Mol Cancer. 2022;21(1):24.
53. Zhang H, et al. CAF secreted miR-522 suppresses ferroptosis and promotes acquired chemo-resistance in gastric cancer. Mol Cancer. 2020;19(1):43.
54. Ren J, et al. Carcinoma-associated fibroblasts promote the stemness and chemoresistance of colorectal cancer by transferring exosomal lncRNA H19. Theranostics. 2018;8(14):3932–48.
55. Arpinati L, et al. From gatekeepers to providers: regulation of immune functions by cancer-associated fibroblasts. Trends Cancer. 2023;9(5):421–43.
56. Tsoumakidou M. The advent of immune stimulating CAFs in cancer. Nat Rev Cancer. 2023;23(4):258–69.
57. Datta J, et al. Combined MEK and STAT3 inhibition uncovers stromal plasticity by enriching for Cancer-Associated fibroblasts with mesenchymal stem cell-like features to overcome Immunotherapy Resistance in Pancreatic Cancer. Gastroenterology. 2022;163(6):1593–612.
58. Desmedt C, et al. Characterization and clinical evaluation of CD10 + stroma cells in the breast cancer microenvironment. Clin cancer Research: Official J Am Association Cancer Res. 2012;18(4):1004–14.
59. Kadota K, et al. Tumoral CD10 expression correlates with aggressive histology and prognosis in patients with malignant pleural mesothelioma. Ann Surg Oncol. 2015;22(9):3136–43.
60. Winner M, et al. Amplification of tumor hypoxic responses by macrophage migration inhibitory factor-dependent hypoxia-inducible factor stabilization. Cancer Res. 2007;67(1):186–93.
61. Sun H, et al. MIF promotes cell invasion by the LRP1-uPAR interaction in pancreatic cancer cells. Front Oncol. 2022;12:1028070.
62. Zhang Y, et al. Adrenomedullin promotes angiogenesis in epithelial ovarian cancer through upregulating hypoxia-inducible factor-1α and vascular endothelial growth factor. Sci Rep. 2017;7:40524.
63. Baba K, et al. Hypoxia-induced ANGPTL4 sustains tumour growth and anoikis resistance through different mechanisms in scirrhous gastric cancer cell lines. Sci Rep. 2017;7(1):11127.
64. Shi H, et al. Transfection of mouse macrophage metalloelastase gene into murine CT-26 colon cancer cells suppresses orthotopic tumor growth,

angiogenesis and vascular endothelial growth factor expression. Cancer Lett. 2006;233(1):139–50.
65. Bhattacharyya S et al. Acidic fibroblast growth factor underlies microenvironmental regulation of MYC in pancreatic cancer. J Exp Med. 2020;217(8).
66. Yuan M, et al. Cancer-associated fibroblasts employ NUFIP1-dependent autophagy to secrete nucleosides and support pancreatic tumor growth. Nat Cancer. 2022;3(8):945–60.

Publisher's Note